Communication-induced multistability and multirhythmicity in a synthetic multicellular system

Qizhi Yi[1,2] and Tianshou Zhou[1,*]

[1]*School of Mathematics and Computational Science, Sun Yat-Sen University, Guangzhou 510275, China*

[2]*School of Mathematics and Information Science, Jiangxi Normal University, Nanchang 330022, China*

(Received 16 November 2010; revised manuscript received 28 February 2011; published 9 May 2011)

Traditionally, the main role of cell-to-cell communication was thought of as synchronizing a population of cells, thereby coordinating cellular behavior. Here we show that cell density, which quantifies cellular communication, can induce multistability and multirhythmicity in a synthetic multicellular system, where individual oscillators are a combination of repressillator and hysteresis-based oscillators and are coupled through a quorum-sensing mechanism. Specifically, for moderately small cell densities, the coupled system can exhibit multistability including stable homogenous and inhomogeneous steady states. For moderately large cell densities, it has the potential to generate multirhythmicity including multimode oscillations such as an in-phase periodic solution, antiphase periodic solution, asymmetric periodic solution, mixed-mode oscillations, coexistence of periodic orbits of several different modes, and bursting oscillations such as periodic bursting, torus quasiperiodic bursting, and chaotic bursting. Such versatility of cell-to-cell communication would be beneficial for cells or organisms to live in diversely changeable environments.

DOI: 10.1103/PhysRevE.83.051907 PACS number(s): 87.18.−h, 05.45.Xt, 87.16.Yc

I. INTRODUCTION

Cell-to-cell communication (CCC) is omnipresent in biological systems ranging from prokaryotes to eukaryotes, and from plants to animals and even to humans [1–5]. In nature, communication is crucial for the physiological functions of diverse organisms; e.g., in bacteria, cells use so-called quorum sensing to communicate with each other through signaling molecules that are released into the cellular environment. By sensing the accumulation of these molecules, bacteria can gauge cell density and coordinate their behavioral response, consequently leading to the formation of various cellular patterns [6]. During development in *Drosophila*, intercellular signaling combines with spatial signal gradient sensing for the formation of vein structure on the wing [7], where a well-defined multicellular pattern emerges from the controlled action of individual cells. In a nervous system, CCC links together a wide variety of cells essential to the functioning of the nervous system within a complex organism, where activity-dependent adenosine-triphosphate (ATP) release by nervous cells acts as an extracellular signal detected by purinergic membrane receptors that modulate intracellular calcium and cyclic adenosine 3′, 5′-monophosphate (AMP) [8]. In each case, CCC plays a role of coordinating population behavior can lead to the formation of a certain cellular pattern [9–11].

CCC systems have attracted great attention for use in synthetic circuits based on genetic components from the virus bacteriophage λ combined with those from the quorum-sensing system. This is mainly because synthetic gene regulatory networks have the potential to enhance our knowledge of cellular processes, on the one hand, and can encourage us to study the design principles of natural systems, on the other. Synthetic networks are also able to display the role of CCC in coordinating multicellular behavior. For example, Garcia-Ojalvo *et al.* [12], showed, by designing a biologically feasible multicellular system, *viz.,* repressilators coupled by quorum sensing, that a diverse and noisy community of interacting repressilators can self-synchronize in a robust way, leading to a substantially improved global rhythmicity in this multicellular system. A similar example by McMillen *et al.* [13] proposed another synthetic gene regulatory network in *E. coli*, which combines the following two features: the system acts as a relaxation oscillator and uses an intercell signaling mechanism to couple individual oscillators. Consequently, the proposed coupling scheme can lead to synchronous behavior across a population of cells, which is achieved through the so-called fast threshold modulation dominant mechanism. Except for such a synchronization function, CCC has other functions; e.g., to study population control and regulated killing, You *et al.* [14] built and characterized a "population control" circuit that autonomously regulates the density of an *E. coli* population. This circuit can set a stable steady state in terms of cell density and gene expression, which is easily tunable by varying the stability of the CCC signal. For more relevant research works, see a recent review paper [15] (including some of references therein), where You *et al.* discussed the dynamic properties of CCC modules, how they can be engineered for synthetic circuit design, and applications of these systems.

We notice that most of the previous relevant works mainly emphasize the role of CCC in synchronizing a population of cells. A natural question is: Can cellular communication induce new dynamics of a multicellular system? The answer is yes; e.g., Basu *et al.* [11] showed that by fusing different fluorescent proteins as outputs of network variants, an initially undifferentiated "lawn" of receivers was engineered to form a bull's eye pattern around a sender colony. Other patterns, such as ellipses and clovers, were also observed by placing senders in different configurations. A more interesting example is that of Ullner *et al.* [16,17], who demonstrated multistability and clustering in a population of repressilators versus phase-repulsive CCC, where the size of coupling strength (i.e., cell density) plays a key role. Recently, we showed that CCC combined with combinatorial regulation can induce several

*mcszhtsh@mail.sysu.edu.cn

dynamic patterns [18,19]. In addition, CCC schemes can even be used to create whole-cell density sensors in biology [20,21]. In spite of this experimental or theoretical endeavor, functions of CCC remain to be fully explored.

This paper further addresses this issue from the viewpoint of dynamics and shows the versatility of CCC in coordinating population behavior. For this, we consider a synthetic multicellular system, where the single oscillator is a combination of a repressillator and a hysteresis-based oscillator, and communication between cells is based on the quorum-sensing mechanism. Such a so-called composite oscillator, which was initially proposed by Yang *et al.* [22], combines two distinct mechanisms into one regulatory network so that only two parameters, the strength of an additional regulatory connection and the timescale separation for one of the variables, control the transition from one mechanism to the other. We demonstrate that cell density, which quantifies cellular communication, can induce multistability and multirhythmicity in coupled composite oscillators. More precisely, small cell densities can make the coupled system exhibit monostability, bistability, or multistability including stable homogenous and inhomogeneous steady states along the route to oscillation death, whereas moderately large cell densities can induce multirhythmicity including multimode oscillations such as in-phase period-1 oscillation, antiphase period-2 oscillation, asymmetric period-2 oscillation (see the following explanations), coexistence of periodic orbits with different oscillation modes such as coexisting in-phase period-1 oscillation and antiphase (or asymmetric) period-2 oscillation, and bursting oscillations such as periodic bursting oscillation, quasiperiodic bursting oscillation, and even chaos. These detailed results indicate that CCC can not only play a role of synchronization but also induce complex yet interesting dynamical phenomena that have not yet been observed in a system of interacting oscillators with a standard coupling (e.g., linear coupling).

II. MODEL

As is well known, the repressillator is an engineered circuit at the transcriptional level, where three repressors [U (TetR), V (CI), and W (LacI)], which are products of three genes [u (*tetR*), v (*cI*), and w (*lacI*), respectively], mutually repress in a cyclic fashion [23] [see Fig. 1(a)]. This circuit can generate self-sustained oscillations. Another synthetic circuit is the hysteresis-based relaxation oscillator [24] [see Fig. 1(b)], where the oscillation mechanism is based on driving a bistable subnetwork of mutually repressing proteins U and V through a hysteresis range of the autoinducer W in concentration. In this circuit, the autoinducer is controlled under a negative feedback from the hysteretic subnetwork, and its dynamics can be made slow by introducing a small parameter in the W equation. As a result, the system generates a relaxation-type oscillation. These two oscillator networks share some similar motifs, which can make it possible to combine the two systems with a few changes. Thus, we can construct a so-called composite oscillator (see Ref. [22] for details); see Fig. 1(c).

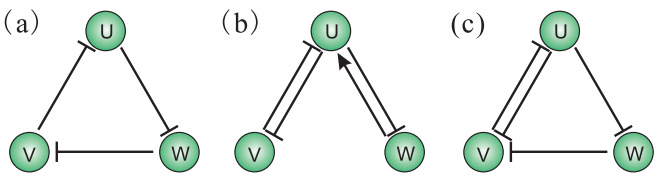

FIG. 1. (Color online) Schematic diagram for three genetic oscillators: (a) repressilator; (b) hysteresis-based relaxation oscillator; (c) composite oscillator.

To establish our model to be studied, we integrate all biological processes such as transcription, translation, promoter binding, etc., into a single step and use the standard quasi-steady-state approximation (QSSA) assumption that dynamics of mRNA molecules is much faster than that of proteins, for simplification. In addition, we define rescaled concentrations as our dynamical variables, and introduce a factor in the W equation into the repressilator so as to be able to slow down dynamics of this component and match the timescale separation used in the relaxation oscillator. Then the resulting equations can be expressed as

$$\begin{aligned} \frac{dU}{dt} &= \frac{\alpha_1}{1+V^n} - U, \\ \frac{dV}{dt} &= \frac{\alpha_1}{1+W^n} + \frac{\alpha_2}{1+U^n} - V, \\ \frac{dW}{dt} &= \varepsilon\left(\frac{\alpha_1}{1+U^n} - W\right), \end{aligned} \tag{1}$$

where dynamics of each component is governed by its synthesis and degradation, which correspond, respectively, to nonlinear functions and negative terms in the right-hand side of Eq. (1). The parameter n is the Hill constant, the dimensionless parameters α_1 and α_2 represent the maximum regulation rates, and the parameter ε describes timescale separation. It has been shown that relaxation-type oscillations occur at $0 < \varepsilon \ll 1$ and in a finite interval of the large α_2, whereas oscillations generated by the original repressilator mechanism do at $\alpha_2 = 0$ and with no timescale separation (i.e., $\varepsilon = 1$). Therefore, the composite oscillator contains both the relaxation-type oscillation mechanism and the repressilator mechanism as its limiting cases, where two key parameters control both oscillatory mechanisms: the strength of U to V connection α_2 and the parameter of timescale separation ε. In addition, there exists a single oscillatory region in the (α_2, ε) phase plane, where the two mechanisms support each other [22].

Next, we introduce a multicellular system based on the above composite oscillator in combination with a quorum-sensing mechanism. In the standard manner of describing such a communication mechanism [12,13,18,19,22,25], small signaling molecules are assumed to diffuse into the inside of each cell in a population and regulate the expression of the target gene. Thus, there are two different kinds of dynamics mechanisms for the signaling molecules: the intracellular signaling molecules that are affected by synthesis, degradation, and diffusion toward or from the intercellular medium, and the extracellular signaling molecules that generally undergo a mixing process in the cellular environment. Let W_i and W_e represent the signaling molecule concentrations within the

inside of cell i and in the cellular environment, respectively. Then the resulting system can be governed by

$$\begin{aligned}\frac{dU_i}{dt} &= \frac{\alpha_1}{1+V_i^n} - U_i,\\ \frac{dV_i}{dt} &= \frac{\alpha_1}{1+W_i^n} + \frac{\alpha_2}{1+U_i^n} - V_i,\\ \frac{dW_i}{dt} &= \varepsilon\left(\frac{\alpha_1}{1+U_i^n} - W_i\right) + \eta\,(W_e - W_i),\end{aligned} \tag{2}$$

where $i = 1,2,\ldots,N$ with N being the total number of cells; the diffusion coefficient η describes the permeability of the cell membrane to the signaling molecules. In the QSSA [12,13,18,19,25], we can write $W_e = \frac{Q}{N}\sum_{i=1}^{N} W_i$, where Q represents cell density, varying between 0 and 1 in a controlled way in a chemostat experiment by changing the total chemostat volume [12]. Our interest is in analyzing what kinds of dynamics the parameter Q can induce if the individual systems are in oscillatory states. In our analysis, Matlab and the Xppaut package [26,27] are used, and $\alpha_1 = 15$, $\alpha_2 = 3.3$, $n = 3$, and $\eta = 2$ are fixed throughout this paper.

It should be pointed out that the value choice of parameters α_1, α_2, n, and η does not change our qualitative result if the single system is guaranteed to generate an oscillation. We will mainly examine two typical cases of ε: large (e.g., $\varepsilon = 0.8$) and small (e.g., $\varepsilon = 0.4$) values, and see how cell density influences the dynamics of a population of composite oscillators.

III. RESULTS

To see how the parameter Q affects collective dynamics of a multicellular system described by the above model (2), we consider only the $N = 2$ case for clarity and simplicity (however, the Appendix shows some results for $N > 2$, which indicate that a larger N does not fundamentally change our qualitative conclusion that CCC can induce multistability and multirhythmicity). Numerical simulations show that the bifurcation diagram of component W versus cell density Q is basically similar when the timescale separation parameter ε is either in the range from 0.5 to 1 (data are not shown) or in the range from 0 to 0.5 (data are also not shown). Moreover, in the former case, the dominant mechanism for oscillations of the uncoupled system can be viewed as the repressilator, whereas in the latter case, the dominant mechanism can be viewed as the relaxation oscillator. Therefore, without loss of generality, we will consider only two cases: $\varepsilon = 0.8$ and $\varepsilon = 0.4$. Two bifurcation diagrams of W versus Q, which correspond to these two values of ε, are shown in Figs. 2(a) and 2(b) (their interpretations will be later given), respectively. In what follows, we will adopt brevities for the explanation of results: PB for pitchfork bifurcation, LP for limit point (i.e., saddle-node point), HB for Hopf bifurcation, PD for period-doubling bifurcation, and TB for torus bifurcation.

Here we simply interpret why the cell density parameter Q can lead to the bifurcation diagrams shown in Fig. 2 . Note that the third equation of Eqs. (2) can be rewritten as the following standard coupling form:

$$\begin{aligned}\frac{dW_i}{dt} &= \varepsilon\left(\frac{\alpha_1}{1+U_i^n} - W_i\right)\\ &\quad -\eta(1-Q)W_i + \frac{Q\eta}{N}\sum_{j=1}^{N}(W_j - W_i).\end{aligned} \tag{3}$$

In this form, the uncoupled system consists of three interrelated equations: the first two equations of Eqs. (2) and Eq. (3) without the coupling term. In general, the coupling term in a standardly coupled system can have a larger influence on collective behaviors (e.g., stability of synchronous states) and less influence on internal dynamics of the single system. Therefore, the cell density parameter Q would greatly affect

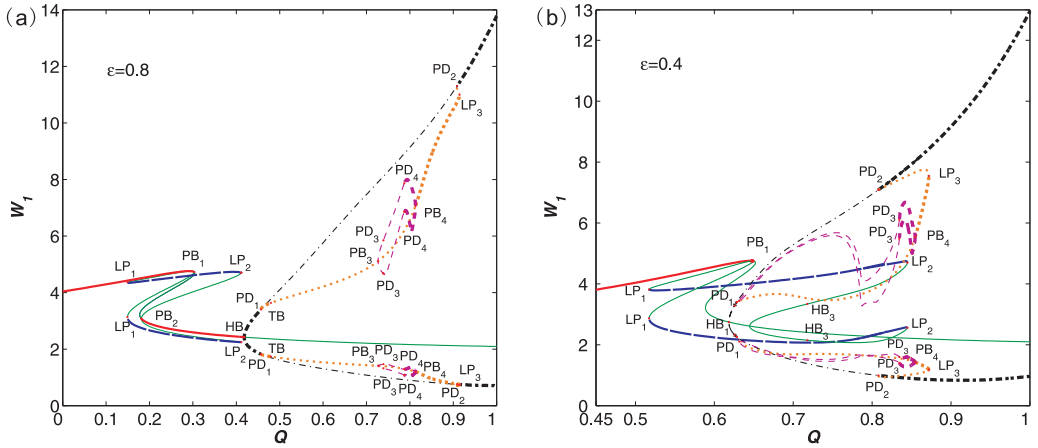

FIG. 2. (Color online) Two bifurcation diagrams of component W versus cell density Q in two coupled composite oscillators: (a) $\varepsilon = 0.8$ and (b) $\varepsilon = 0.4$. In both diagrams, thick solid lines stand for two different stable homogeneous steady states; thick long dashed lines for stable inhomogeneous steady states; thin solid lines for unstable steady states; thick dash-dotted lines for stable in-phase period-1 oscillations; thin dash-dotted lines for unstable period-1 oscillations; thick dotted lines for stable antiphase period-2 oscillations; and thin dotted lines for unstable antiphase period-2 oscillations. Note that a segment of the thick solid line for $Q \in (0,0.45)$ in (b) is omitted for better exhibition. See the main text for the meanings of abbreviated symbols in the two diagrams.

dynamics and even can induce new dynamics of the currently uncoupled system since it depends obviously on Q [see Eq. (3)].

A. Multistability

First, we point out that the individual system can exhibit oscillations for arbitrary $\varepsilon \in (0,1)$ and fixed $\alpha_1 = 15$, $n = 3$, and $\eta = 2$ as long as α_2 is appropriately chosen (data are not shown here). In particular, it is oscillatory for both $\alpha_2 = 3.3$ (which will be fixed in the following analysis) and $\varepsilon = 0.8$ or 0.4. Then, we mainly examine two cases of ε: large (e.g., $\varepsilon = 0.8$) and small (e.g., $\varepsilon = 0.4$) values, and see how the cell density parameter Q influences steady states of the coupled system and their stability while the individual system is in an oscillatory state.

For $\varepsilon = 0.8$, we observe from Fig. 2(a) that because of two subcritical pitchfork bifurcations at PB_1 and PB_2, the coupled system has two different stable homogeneous steady states if Q locates, respectively, in an interval bounded by the W axis and PB_1 and in another interval bounded by PB_2 and HB (see upper and below thick solid curves). Here, by homogeneous steady state (HSS), we mean that two corresponding components in the coupled system take the same value. With the increase of Q from the value corresponding to LP_1, saddle-node bifurcations occurring at two limit points, LP_1 and LP_2, lead to the appearance of stable inhomogeneous steady states, which can persist in the interval bounded by LP_1 and LP_2 (see long dashed curves). Here, by inhomogeneous steady state (IHSS), we mean that two corresponding components in the coupled system take different values. Then, when Q is beyond the value corresponding to LP_2, the IHSS disappears but the low HSS still persists even until other complex oscillatory behaviors arise (see low thick solid curve). In addition, we observe the coexistence of two stable steady states: IHSS and upper or lower HSS (see thick long dashed and thick solid curves between LP_1 and PB_2 or between PB_1 and LP_2), or the coexistence of three stable steady states: two HSSs and one IHSS (see thick solid and thick long dashed curves between PB_2 and PB_1) when Q takes moderately small values. Specifically, the coupled system has the unique HSS and is therefore monostable if Q is in the interval bounded by the W axis and LP_1, has both a HSS and an IHSS, and is therefore bistable if Q is in the interval bounded by LP_1 and PB_2 or by PB_1 and LP_2, and displays multistability due to the coexistence of three stable steady states: two HSSs and one IHSS, if Q is in the interval bounded by PB_2 and PB_1. The above analysis indicates that the coupled system can undergo transitions from monostability to bistability and to multistability if Q increases from 0 to PB_1 through LP_1 and PB_2, and returns to a monostable state via a bistable state if Q is beyond the value corresponding to PB_1. Note that in the coexistence case of stable steady states, to which state the coupled system ultimately evolves depends on the choice of initial conditions.

For $\varepsilon = 0.4$, the situation is somewhat different in contrast to $\varepsilon = 0.8$ [compare Fig. 2(b) with Fig. 2(a)]. The main differences are that the range of Q for the unique stable steady state in the case $\varepsilon = 0.8$ is currently enlarged, and one of two homogeneous steady states in the case $\varepsilon = 0.8$ has currently disappeared [compare thick solid curves in Fig. 2(a) and Fig. 2(b)].

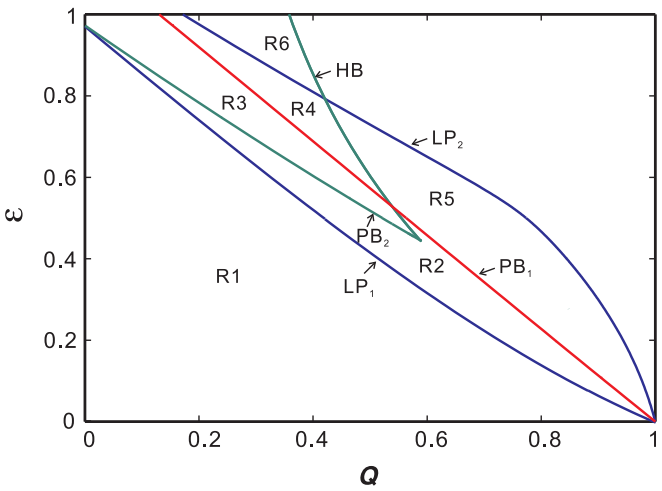

FIG. 3. (Color online) Distributed regions of stable steady states in the (Q, ε) phase plane. The curves are, respectively, the loci of five bifurcation points marked in Fig. 2: LP_1, PB_2, PB_1, HB, and LP_2, which partition the whole parameter region into six subregions with each corresponding to one of the emerging HSS and IHSS or their different combinations: R1 for HSS_1; R2 for HSS_1 and IHSS; R3 for HSS_1, HSS_2, and IHSS; R4 for HSS_2 and IHSS; R5 for IHSS; and R6 for HSS_2.

In both cases, the coexistence of stable steady states follows two kinds of bifurcations: PB and LP, which have been marked in Fig. 2. It is worth noting that the emergence of stable steady states in the coupling case implies oscillation death in the individual system. In addition, some of the stable steady states can also coexist with some periodic orbits (data are not shown here but are partially mentioned in the caption of Fig. 2).

Next, we demonstrate distributed regions of stable steady states in the (Q, ε) parameter phase plane (see Fig. 3), which can further enhance our understanding of communication-induced multistability (including bistability). First, Fig. 3 indicates that ε also has important influence on the formation of stable steady states and their stability in the coupled system. Second, the united effect of ε and Q can lead to the situation that stable steady states are distributed mainly in six subregions, denoted by R1–R6. There exist HSS_1 [where the subscript 1 represents a high state in the (U,V) state space] in R1, HSS_1 and IHSS in R2, HSS_1, HSS_2 and IHSS in R3 [where the subscript 2 represents a low state in the (U,V) state space], HSS_2 and IHSS in R4, IHSS in R5, and HSS_2 in R6. It should be pointed out that the $R2$ and $R5$ regions would contain other types of attractors such as oscillations, which can moreover coexist with both IHSS and HSS_1 or with IHSS (see below for more details).

B. Multirhythmicity

Let us introduce or explain several terms used in the following analysis before presenting our results. The period-1 oscillation means that there are one maximum and one minimum, whereas the period-2 oscillation means that there are two local maxima and two local minima [28]. By multirhythmicity, we mean the following three classes of behaviors: multimode

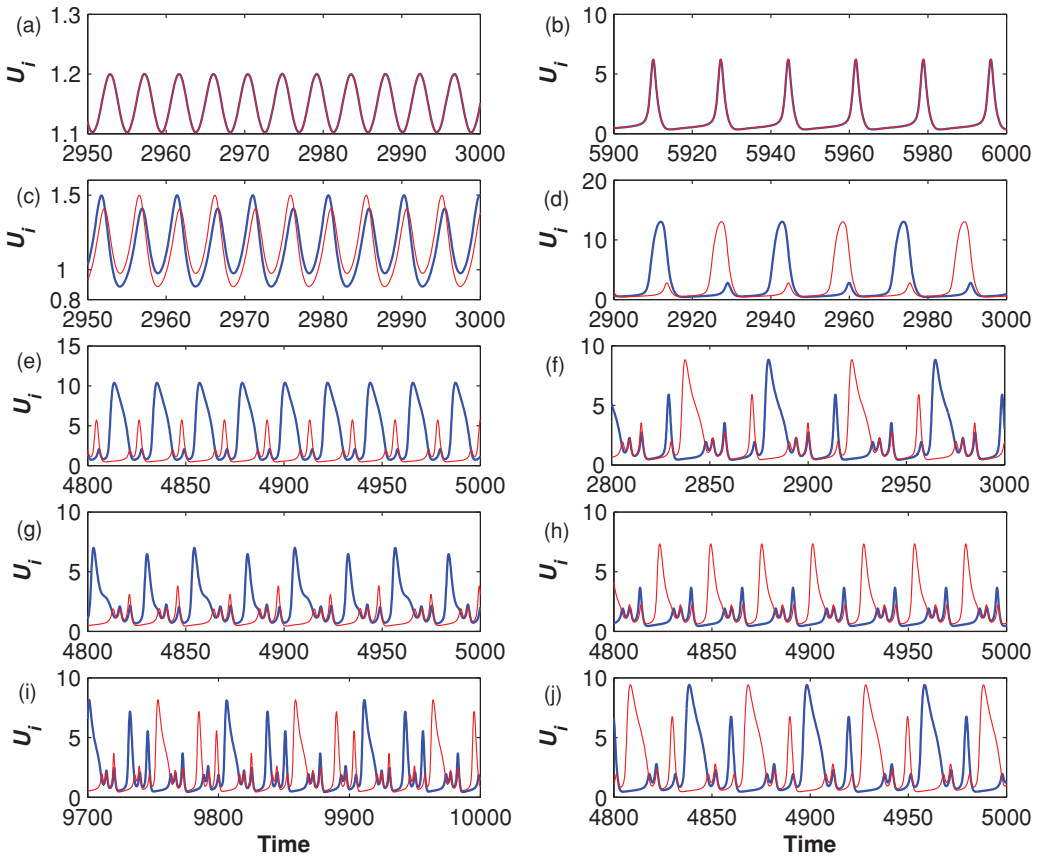

FIG. 4. (Color online) Cell density-induced multimode oscillations in two coupled composite oscillators with $\varepsilon = 0.8$: (a)–(b) two modes of in-phase period-1 oscillations for $Q = 0.42$ and $Q = 0.93$; (c)–(d) two modes of period-2 oscillations with a shifted phase for $Q = 0.47$ and $Q = 0.91$; (e) asymmetric period-2 oscillation for $Q = 0.80$; (f)–(j) five types of mixed-mode oscillations (MMOs): (f) symmetric $1^2 1^2 1^1$ MMO for $Q = 0.766$, (g) asymmetric $1^2 1^2$ MMO for $Q = 0.73$; (h) asymmetric 1^2 MMO for $Q = 0.745$, (i) symmetric $1^2 1^1 1^2 1^3$ MMO for $Q = 0.76$, and (j) symmetric $1^1 1^3$ MMO for $Q = 0.78$.

oscillations, coexistence of different-mode oscillations, and bursting oscillations. Multimode oscillations can further be divided into symmetric and asymmetric oscillations according to characteristics of oscillation amplitude, but also can further be divided into period-1, period-2, and mixed-mode oscillations according to the wave form of oscillation. Here, by symmetric oscillation we mean that two subsystems oscillate with the same amplitude but may allow a phase difference between them (in particular, no phase difference corresponds to in-phase oscillation, whereas the half-period phase difference corresponds to antiphase oscillation). In contrast, asymmetric oscillation means that there are differences in amplitude between two oscillators, i.e., the oscillation exhibits asymmetry in amplitude. Mixed-mode oscillations are a complex type of dynamics, which can be a mixture of small-amplitude oscillations and large-amplitude (relaxation) excursions. In general, a mixed-mode periodic orbit can be characterized by the so-called Farey sequence of the form $L_0^{k_0} L_1^{k_1} \ldots L_j^{k_j}$, which encodes the number of large-amplitude excursions (denoted by L_j) and the number of small-amplitude oscillations (denoted by k_j), respectively [29]. We point out that such a kind of oscillation has been observed in both experiments and theoretical models involved in neuroscience, chemistry, and so on [29–31]. Finally, bursting oscillations can further be divided into three cases: periodic, quasiperiodic, and chaotic bursting. We point out that these kinds of bursting oscillations have been observed in neural activity, pancreatic β cells, and metabolic or genetic control networks [32–34].

Now we will focus on examining how the cell density parameter Q leads to multirhythmicity. First, we observe from the above bifurcation diagrams that Q can make the coupled system undergo a Hopf bifurcation, but its location depends on the size of the timescale separation parameter ε; e.g., it is increasing with the decrease of ε [compare Fig. 2(a) with Fig. 2(b)]. However, the behavior produced through the bifurcation is different when ε takes a large value and a small value, respectively: The former makes the coupled system generate a stable limit cycle, whereas the latter makes it generate an unstable limit cycle. Second, a new branch beginning from PD_1 emerges on each of two branches of the original periodic orbit produced through the Hopf bifurcation, forming a period-2 limit cycle (see the change of Q from small to large values in Fig. 2). For example, for $\varepsilon = 0.8$, the coupled system goes through torus bifurcation at TB, pitchfork bifurcation at PB_4, and saddle-node bifurcation at LP_3 in order and achieves a stable antiphase period-2 limit cycle. In contrast, for $\varepsilon = 0.4$, it undergoes pitchfork bifurcation at PB_4 and saddle-node bifurcation at LP_3 in order, and achieves a

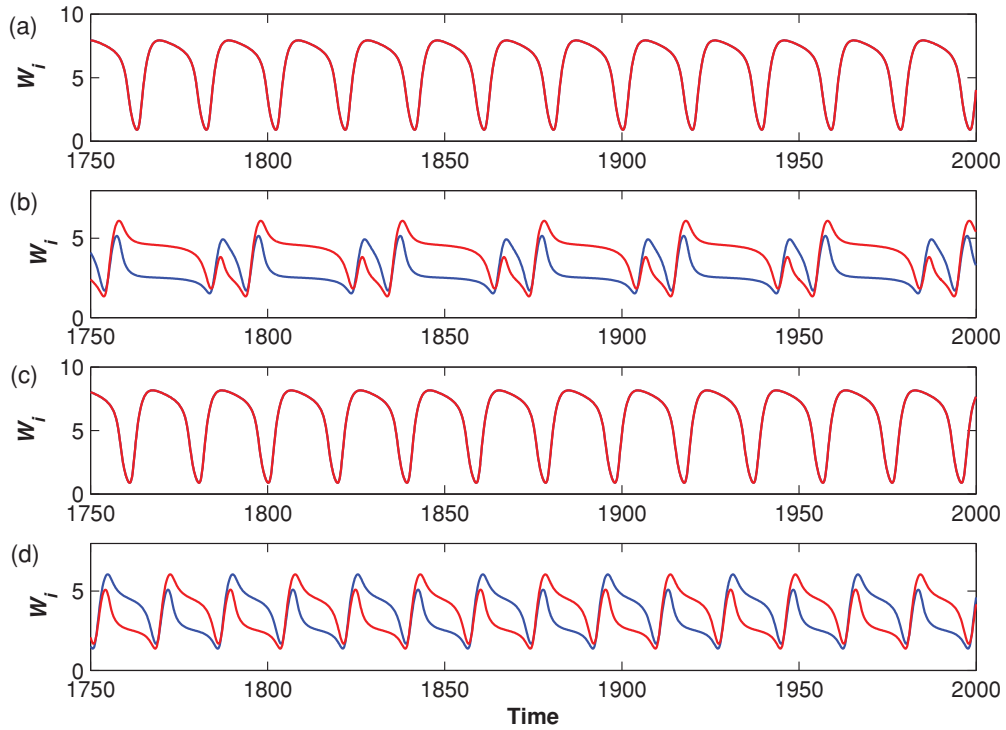

FIG. 5. (Color online) Observed coexisting attractors in the two coupled composite oscillators with $\varepsilon = 0.4$: (a)–(b) coexisting in-phase period-1 and asymmetric period-2 oscillations for $Q = 0.85$; (c)–(d) coexisting in-phase period-1 and antiphase period-2 oscillations for $Q = 0.86$.

stable antiphase period-2 limit cycle. Furthermore, on each of two new branches bifurcated from PD_1 until LP_3, the coupled system undergoes more complex bifurcations and produces a stable asymmetric period-2 limit cycle between PD_4 and PB_4 for $\varepsilon = 0.8$ or between PD_3 and PB_4 for $\varepsilon = 0.4$. Third, bifurcations are more complex in the case of small ε values than those in the case of large ε values, implying that the relaxation oscillator is more easily influenced by CCC than the repressilator. In particular, there exists a certain range of Q such that several different behaviors can coexist, but the coexistence mode (e.g., coexisting steady states and periodic orbits, or coexisting periodic orbits) is more complex in the latter case than in the former case.

Next, we show more details on communication-induced multirhythmicity by distinguishing three cases: multimode oscillations, coexistence of different-mode oscillations, and bursting oscillations.

First, Fig. 4 shows several interesting but typical multimode oscillations including in-phase oscillation, antiphase oscillation, and several types of mixed-mode oscillations. Specifically, for moderately small or large Q, the coupled system can exhibit two modes of in-phase period-1 oscillation; see Figs. 4(a) and 4(b). Moreover, the period of the former is smaller than that of the latter, indicating that the cell density can change oscillation period. In addition, the oscillation with this mode is actually the usual synchronization observed in a system of standardly coupled oscillators. Similarly, for moderately small or large Q, we can observe two modes of antiphase period-2 oscillation; see Figs. 4(c) and 4(d). In these modes, the oscillation is characterized by two different amplitudes, small and large, but the higher peak between two oscillators differs by half a period. When Q decreases from a large value, an asymmetric periodic oscillation can arise, e.g., an asymmetric period-2 oscillation appears for $Q = 0.8$; see Fig. 4(e). With the further decrease of Q, several types of mixed-mode oscillations can be observed, e.g., $1^2 1^2 1^1$ state for $Q = 0.766$, $1^2 1^2$ state for $Q = 0.73$, 1^2 state for $Q = 0.745$, $1^2 1^1 1^2 1^3$ state for $Q = 0.76$, and $1^1 1^3$ state for $Q = 0.78$; see Figs. 4(f)–4(j), respectively. Such mixed-mode oscillations have been observed in other dynamical systems [29–31].

Next, we show the coexistence of periodic oscillations with different modes. As an example, Fig. 5 shows the coexistence of two different types of oscillations: in-phase period-1 and asymmetric period-2 oscillations for $\varepsilon = 0.4$ and $Q = 0.85$, and in-phase period-1 and antiphase period-2 oscillations for $\varepsilon = 0.4$ and $Q = 0.86$. In addition, there are other types of coexistence phenomena, e.g., coexisting IHSS and antiphase period-2 oscillation for $\varepsilon = 0.7$ and $Q = 0.49$, coexisting IHSS and in-phase period-1 oscillation for $\varepsilon = 0.4$ and $Q = 0.82$, and coexisting IHSS, in-phase period-1 oscillation and asymmetric period-2 oscillation for $\varepsilon = 0.4$ and $Q = 0.84$ (data not shown). Note that three points, $(Q,\varepsilon) = (0.49,0.7)$, $(0.82,0.4)$, and $(0.84,0.4)$, are located in the R5 region of Fig. 3. More complex coexistence phenomena are possible in this region.

Finally, we simply demonstrate an interesting kind of phenomenon: communication-induced bursting oscillations, which are often observed in neuron activity (see Ref. [32] and references therein). Figure 6 shows three types of bursting oscillations: periodic bursting [Fig. 6(a)], quasiperiodic

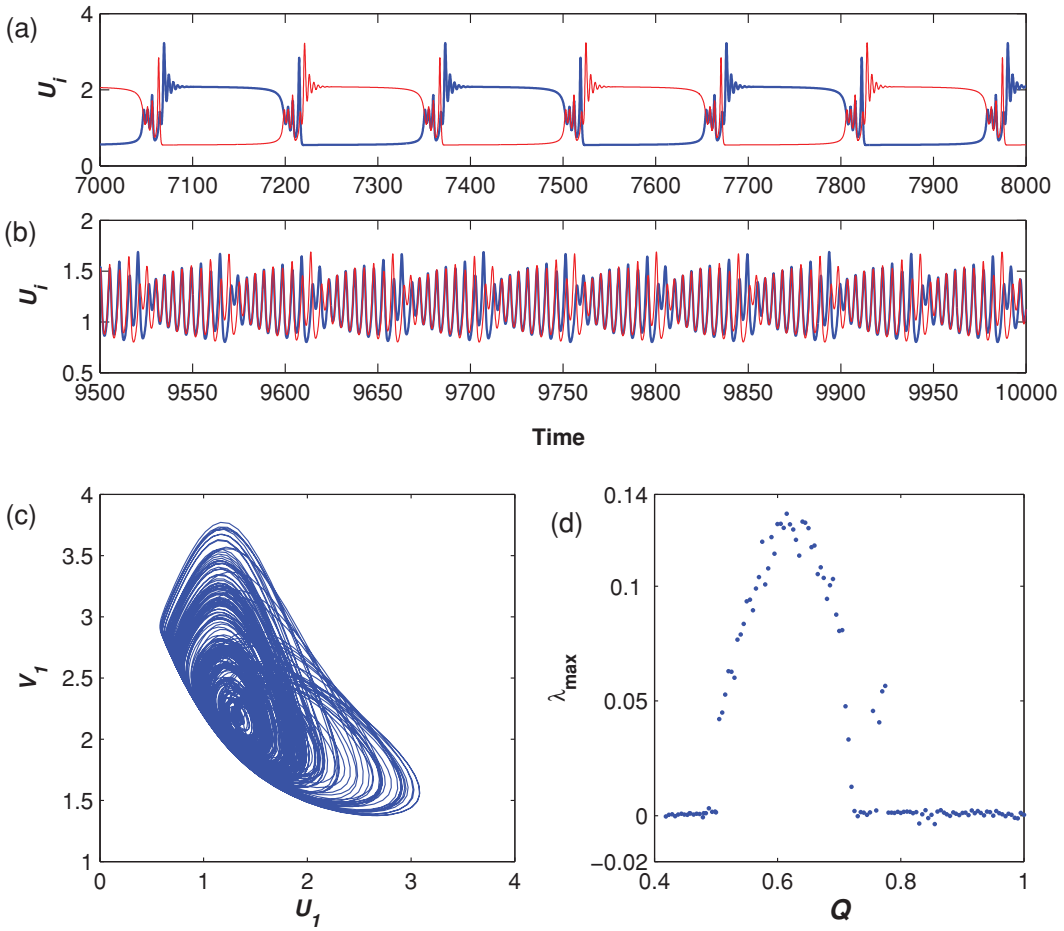

FIG. 6. (Color online) Three observed modes of bursting oscillation in the two coupled composite oscillators: (a) periodic bursting oscillation when $\varepsilon = 0.6$ and $Q = 0.664$; (b) quasiperiodic bursting oscillation when $\varepsilon = 0.8$ and $Q = 0.49$; (c)–(d) chaotic bursting oscillation when $\varepsilon = 0.8$ and $Q = 0.60$, where (c) is the phase diagram and (d) shows the maximal Lyapunov exponent λ_{max} versus cell density Q.

bursting [Fig. 6(b)] and chaotic bursting [Fig. 6(c)–6(d)]. The occurrence of quasiperiodic bursting oscillation is due to torus bifurcation. In Fig. 6(c)– 6(d), to verify the existence of chaotic attractors, we also show the dependence relationship of the maximal Lyapunov exponent(λ_{max}) on cell density Q. Apparently, there is a small interval of Q centered at $Q = 0.6$ such that λ_{max} is positive, implying that the coupled system is indeed chaotic. However, at other ranges of Q, the maximal Lyapunov exponent drops to zero. In addition, numerical simulations show that the chaotic regime contains some periodic windows, which are actually mixed-mode oscillations; see Figs. 4(f)– 4(j). Moreover, the mechanism of generating chaos is through a quasiperiodic path (data not shown).

IV. CONCLUSION AND DISCUSSION

For a multicellular system, communication between cells is commonly seen, in particular in bacteria. Such communication not only is crucial for the physiological functions of diverse organisms from the viewpoint of biology but also plays a key role in coordinating population behavior from the viewpoint of dynamics. In addition, its role is also reflected in antiquorum-sensing strategies present in both bacteria and eukaryotes, which are apparently designed to combat bacteria that depend on CCC for successful adaption to particular niches [1]. However, because of complexity in communication mechanisms and functions, the functions of CCC remain to be fully understood. Here we have from the viewpoint of dynamics shown the versatility of CCC in coordinating population behavior by considering a synthetic multicellular system, which is composed of composite oscillators coupled to a quorum-sensing mechanism. It can synchronize a population of composite oscillators, on the one hand, and can simultaneously induce complex dynamical behaviors including multistability and multirhythmicity as well as coexistence as shown in this paper, on the other. Such versatility would be beneficial as cells face diversely changeable environments.

That we have selected the composite oscillator for investigation is based mainly on the fact that such an oscillator can combine two typical oscillation mechanisms: the repressilator and the relaxation oscillator. Therefore, we can show as many as possible functions of CCC. Moreover, according to our investigation, we have actually shown the versatility of CCC in the two typical-oscillation cases since the repressilator and the relaxation oscillator can be taken as the limit of the composite

oscillator in a sense. In addition, we have shown that CCC has more influence in the relaxation oscillator case than in the repressilator case, but our previous work showed that the former is less sensitive (or more robust) to noise than the latter [35].

However, it should be pointed out that our model is simplified in several aspects. First, we neglected some detailed biological processes such as transcription, translation, and promoter binding, and instead integrated them into a single step. In particular, our model did not consider the effect of combinatorial regulation that can be described by several kinds of *cis*-regulatory input functions [36–38]. In fact, it has been shown that the combinatorial regulation also has important influence on the formation of cellular patterns [18,19]. Second, to simplify our multicellular system model, we adopted the mean-field approximation for the signaling molecule concentrations in the extracellular environment. Third, we neglected some biological factors such as cellular diversity, time delays existing during signaling transmission between cells, and stochastic fluctuations, which would also have significant influence on dynamics of coupled systems. In fact, some studies including experimental and theoretical works have shown some influence [39–44]. Thus, our next work will focus on effects of ways of communication (e.g., bidirectional or unidirectional communication), various biological processes, biological factors, and so on.

ACKNOWLEDGMENTS

This work was supported by the Natural Science Key Foundation of the People's Republic of China (No. 60736028), the Natural Science Foundation of the People's Republic of China (No. 30973980 and 11005162), 973 Project of China (No. 2010CB945400), and Distinguished Young Talents in Higher Education of Guangdong, China (Grant No. LYM10074).

APPENDIX

1. In the case $N > 2$

In the main text, we have shown that cell-to-cell communication can induce multistability and multirhythmicity in the case of two coupled oscillators. Here we will show that the number of oscillators does not change this qualitative conclusion. For this, we perform a direct numerical simulation for a middle-scale coupled system (e.g., the number of oscillators is set as $N = 20$) and compare the results in the case $N = 2$ with those in the case $N = 20$. In simulation, we fix a set of parameter values, where all the parameters except for the cell density $Q \in [0,1]$ are given in the main text, and randomly generate initial values of three proteins U, V, and W using a uniform distribution in the range $[0,2]$ so as to obtain 200 sets of time series data for one component of coupled oscillators in the $N = 2$ and 20 cases, respectively. Then we count the number of each of three classes of stable attractors: homogeneous steady state (HSS), inhomogeneous steady state (IHSS), and oscillation based on these data for both cases. Thus, we are able to detect each stable attractor with a significant attracting basin and further obtain the dependence of the number of stable regions on Q (see Fig. 7, where $\varepsilon = 0.8$ is fixed).

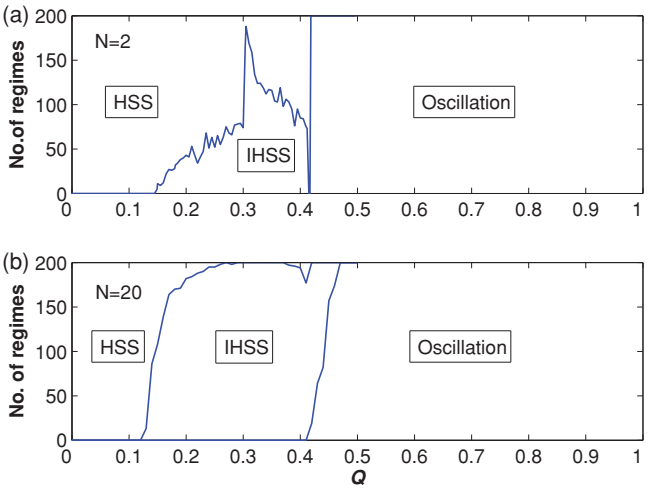

FIG. 7. (Color online) Shown is that the system size has only finite influence on the distribution of dynamical regions in the case $\varepsilon = 0.8$. When the cell density changes in the $(0,1)$ interval, there are three dynamical regions: HSS, IHSS, and oscillation, in each case $N = 2$ (a) and $N = 20$ (b), but the boundary of these regions is somewhat different between the two cases (compare boundaries of the IHSS region in two diagrams), implying that the system size influences only coexistent regions but does not alter the qualitative conclusion that cellular communication can induce multistability and multirhythmicity.

Comparing Fig. 7(a) with Fig. 7(b), we find that the two cases share basically the same dynamical characteristics: Each coupled system can exhibit monostability due to the existence of HSS when Q is appropriately small, multistability (including bistability) due to the coexistence of HSS and IHSS when Q is suitably large, and oscillation when Q is large enough, but also there are some differences between two cases. One difference is that increasing the system size from $N = 2$ to 20 can enlarge the stable region for IHSS, and both oscillation and IHSS can coexist. Another difference is that in the coupled system with $N = 20$ can have parameter regions where multiple IHSSs can coexist, mainly due to the fact that N coupled oscillators have $N - 1$ different distributions between the steady-state clusters. Specifically, consider some component in the coupled system, e.g., $U_i (i = 1,2,\ldots,N)$. Assume that mU are located at a higher concentration state (denoted by mU), whereas the remaining $(N - m)$ U are at a lower concentration state [denoted by $(N - m)L$], where m can take a value between 1 and $N - 1$. We denote such an IHSS mode as $mU|(N - m)L$. As an example, Fig. 8(a)–(d) displays four coexisting modes of IHSSs with different distributions for $Q = 0.36$: $10U|10L$, $9U|11L$, $8U|12L$, and $7U|13L$, respectively. Note that for different Q, IHSSs of different modes can coexist (data not shown).

More numerical simulations show that the coupled system with $N = 20$ and $\varepsilon = 0.8$ can exhibit communication-induced multirhythmicity similar to that shown in Figs. 4 and 6, including multimode oscillations, e.g., two modes of in-phase period-1 oscillations [see Fig. 8(e) for one of them], two modes of antiphase period-2 oscillations [see Fig. 8(f) for one of them], and asymmetric period-2 oscillation [see Fig. 8(g)]; several types of mixed-mode oscillations, e.g., symmetric

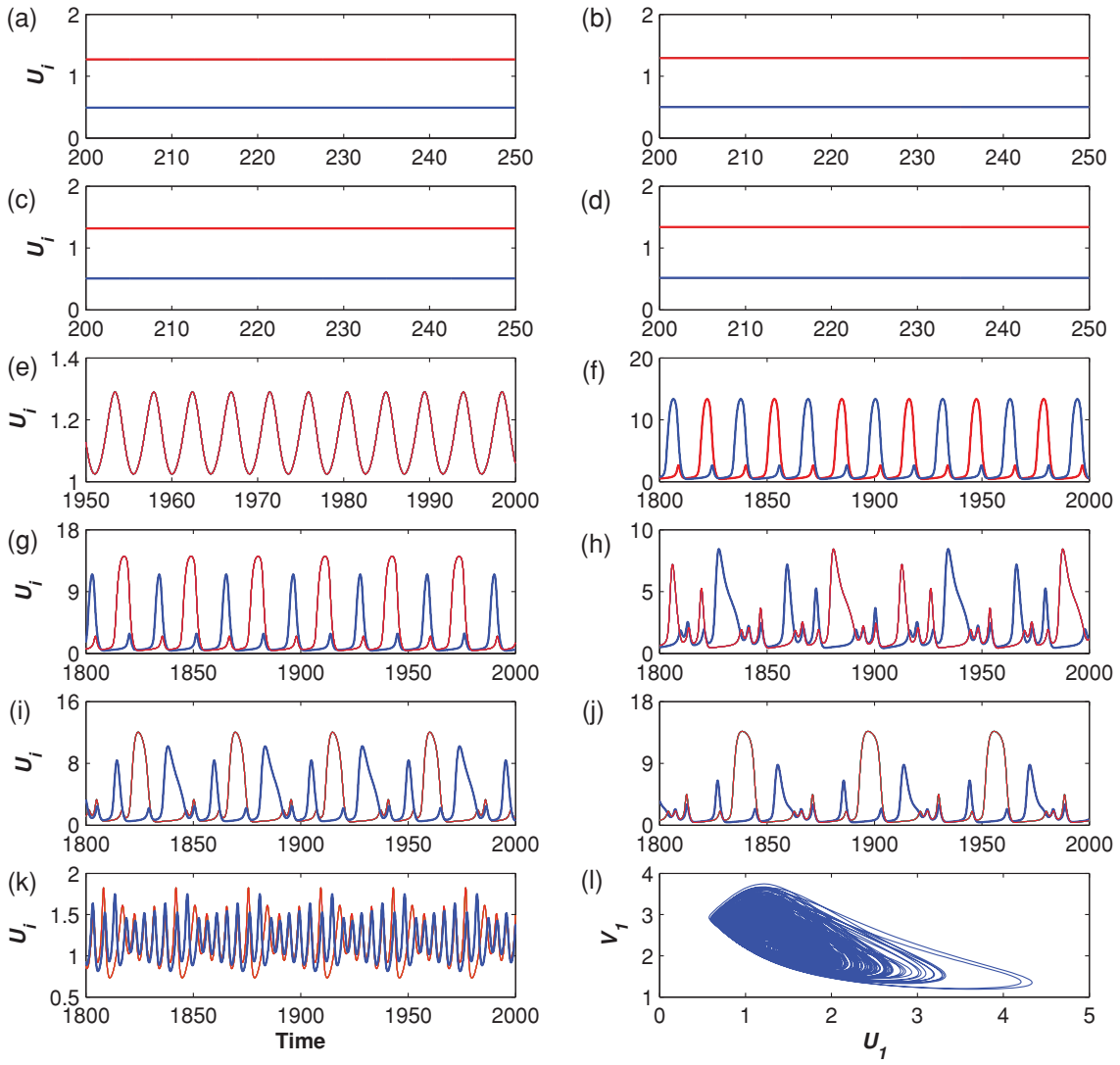

FIG. 8. (Color online) An example for communication-induced multistability and multirhythmicity in 20 coupled composite oscillators with $\varepsilon = 0.8$: (a)–(d) four modes of coexisting IHSSs with different distributions for $Q = 0.36$: (a) $10U|10L$, (b) $9U|11L$, (c) $8U|12L$, (d) $7U|13L$; (e)–(j) multimode oscillations: (e) in-phase period-1 oscillation for $Q = 0.43$, (f)–(g) antiphase period-2 oscillation and asymmetric period-2 oscillation for $Q = 0.9$, (h)–(j) three types of MMOs: (h) symmetric $1^2 1^1 1^2 1^3$ MMO for $Q = 0.76$, (i) asymmetric $1^1 1^1$ MMO for $Q = 0.82$, and (j) asymmetric $1^2 1^1$ MMO for $Q = 0.82$; (k)–(l) two modes of bursting oscillations, where (k) corresponds to quasiperiodic bursting for $Q = 0.51$, and (l) to chaotic bursting for $Q = 0.6$.

$1^2 1^1 1^2 1^3$ MMO for $Q = 0.76$ [see Fig. 8(h)], asymmetric $1^1 1^1$ MMO for $Q = 0.82$ [see Fig. 8(i)], and asymmetric $1^2 1^1$ MMO for $Q = 0.82$ [see Fig. 8(j)]; and bursting oscillation, e.g., quasiperiodic bursting oscillation [see Fig. 8(k)] and chaotic bursting oscillation [see Fig. 8(l)]. However, the coupled system can also demonstrate the coexistence of several periodic oscillations different from that in the case $N = 2$, e.g., coexisting antiphase period-2 and asymmetric period-2 oscillations for $Q = 0.9$, and coexisting asymmetric $1^1 1^1$ MMO and asymmetric $1^2 1^1$ MMO for $Q = 0.82$, which have not been observed in the case $N = 2$ for all $Q \in [0,1]$. In addition, we also find many other periodic oscillation modes and coexisting modes of periodic oscillations (data not shown).

In summary, we have seen that increasing the number of oscillators does not change the qualitative conclusion of communication-induced multistability and multirhythmicity but possibly leads to richer phenomena.

2. More results on the coexistence of several different behaviors

In the main text, we have shown some coexisting phenomena. Here we show more coexisting phenomena. For clarity, we examine several lines of the timescale separation parameter in Fig. 3 and list some ranges of the cell density parameter and the corresponding states, including the ranges for the existence of stable steady states, in-phase period-1 oscillations, antiphase and asymmetric period-2 oscillations, and those for the coexistence of several different dynamical behaviors, as follows:

(1) For $\varepsilon = 0.8$, HSS_1 in (0,0.3036); HSS_2 in (0.1813,0.4186); IHSS in (0.1493,0.4119);

IPPOO in $(0.4186,0.457)\bigcup(0.9089,1)$; APPTO in $(0.457,0.4798)\bigcup(0.8131,0.9145)$; and ASPTO in $(0.7873,0.8131)$.

(2) For $\varepsilon = 0.7$, HSS_1 in $(0,0.3901)$; HSS_2 in $(0.2905,0.4569)$; IHSS in $(0.2376,0.5373)$; IPPOO in $(0.4569,0.4791)\bigcup(0.8787,1)$; APPTO in $(0.4791,0.4961)\bigcup(0.8159,0.8926)$; and ASPTO in $(0.7905,0.8159)$.

(3) For $\varepsilon = 0.6$, HSS_1 in $(0,0.4767)$; HSS_2 in $(0.4035,0.5019)$; IHSS in $(0.3278,0.6638)$; IPPOO in $(0.5019,0.5124)\bigcup(0.8506,1)$; APPTO in $(0.5124,0.5239)\bigcup(0.8225,0.8759)$; and ASPTO in $(0.7977,0.8225)$.

(4) For $\varepsilon = 0.5$, HSS_1 in $(0,0.5633)$; HSS_2 in $(0.5212,0.555)$; IHSS in $(0.4207,0.7736)$; IPPOO in $(0.555,0.5605)\bigcup(0.8259,1)$; APPTO in $(0.5605,0.5746)\bigcup(0.8345,0.868)$; and ASPTO in $(0.811,0.8345)$.

(5) For $\varepsilon = 0.4$, HSS_1 in $(0,0.65)$; IHSS in $(0.5173,0.8447)$; IPPOO in $(0.8078,1)$; APPTO in $(0.8546,0.8791)$; and ASPTO in $(0.8346,0.8546)$.

Here the following abbreviated symbols are used: HSS for homogeneous steady state; IHSS for inhomogeneous steady state; IPPOO for in-phase period-one oscillation; APPTO for antiphase period-two oscillation; ASPTO for asymmetric periodic-two oscillation. The subscript 1 stands for a high state, whereas the subscript 2 stands for a low state in the (U, V) state space.

From the above list, we can find that there are intervals of coexisting phenomena, e.g., the IPPOO can coexist with APPTO in the interval (0.9089, 0.9145), and HSS_1 can coexist with HSS_2 in the interval (0.1813, 0.3036) and with IHSS in the interval (0.1493, 0.3036), for the fixed $\varepsilon = 0.8$. For other values of ε, there are some similar existing phenomena.

[1] M. E. Taga and B. L. Bassler, Proc. Natl. Acad. Sci. USA **100**, 14549 (2003).
[2] J. Golden and H. Yoon, Curr. Opin. Microbiol. **1**, 623 (1998).
[3] M. Heinlein, Curr. Opin. Plant Biol. **5**, 543 (2002).
[4] M. Yamaguchi, E. Yoshimoto, and S. Kondo, Proc. Natl. Acad. Sci. USA **104**, 4790 (2007).
[5] M. Fussenegger, Nature (London) **463**, 301 (2010).
[6] B. L. Bassler and R. Losick, Cell **125**, 237 (2006).
[7] S. S. Blair, Annu. Rev. Cell Dev. Biol. **23**, 293 (2007).
[8] R. D. Fields and G. Burnstock, Nat. Rev. Neurosci. **7**, 423 (2006).
[9] R. Scherrer and V. Shull, Can. J. Microbiol. **32**, 607 (1986).
[10] E. Ben-Jacob, I. Cohen, O. Shochet, A. Tenenbaum, A. Czirok, and T. Vicsek, Phys. Rev. Lett. **75**, 2899 (1995).
[11] S. Basu, Y. Gerchman, C. H. Collins, F. H. Arnold, and R. Weiss, Nature (London) **434**, 1130 (2005).
[12] J. Garcia-Ojalvo, M. B. Elowitz, and S. H. Strogatz, Proc. Natl. Acad. Sci. USA **101**, 10955 (2004).
[13] D. McMillen, N. Kopell, J. Hasty, and J. J. Collins, Proc. Natl. Acad. Sci. USA **99**, 679 (2002).
[14] L. C. You, R. Sidney Cox III, R. Weiss, and F. H. Arnold, Nature (London) **428**, 868 (2004).
[15] A. Pai, Y. Tanouchi, C. H. Collins, and L. C. You, Curr. Opin. Biotechn. **20**, 461 (2009).
[16] E. Ullner, A. Zaikin, E. I. Volkov, and J. García-Ojalvo, Phys. Rev. Lett. **99**, 148103 (2007).
[17] E. Ullner, A. Koseska, J. Kurths, E. Volkov, H. Kantz, and J. García-Ojalvo, Phys. Rev. E **78**, 031904 (2008).
[18] Q. Z. Yi, J. J. Zhang, Z. J. Yuan, and T. S. Zhou, Eur. Phys. J. B **75**, 365 (2010).
[19] J. J. Zhang, Z. J. Yuan, and T. S. Zhou, Phys. Rev. E **79**, 041903 (2009).
[20] H. Kobayashi *et al.*, Proc. Natl. Acad. Sci. USA **101**, 8414 (2004).
[21] T. S. Gardner, C. R. Cantor, and J. J. Collins, Nature (London) **403**, 339 (2000).
[22] D. Yang and A. Kuznetsov, Chaos **19**, 033115 (2009).
[23] M. Elowitz and S. Leibler, Nature (London) **403**, 335 (2000).
[24] J. Hasty, F. Isaacs, M. Dolnik, D. McMillen, and J. J. Collins, Chaos **11**, 207 (2001).
[25] T. S. Zhou, J. J. Zhang, Z. J. Yuan, and L. N. Chen, Chaos **18**, 037126 (2008).
[26] B. Ermentrout, *Simulating, Analyzing and Animating Dynamical Systems: A Guide to Xppaut for Researchers and Students (Software, Environment and Tools)* (SIAM Press, Philadephia, PA, 2002).
[27] B. Ermentrout, [http://www.math.pitt.edu/∼bard/xpp/xpp.html].
[28] R. Laje and G. B. Mindlin, Phys. Rev. Lett. **89**, 288102 (2002).
[29] M. Krupa, N. Popovic, N. Kopell, and H. G. Rostein, Chaos **18**, 015106 (2008).
[30] C. A. Negro, C. G. Wilson, R. J. Butera, H. Rigatto, and J. C. Smith, Biophys. J. **82**, 206 (2002).
[31] V. Petrov, S. K. Scott, and K. Showalter, J. Chem. Phys. **97**, 6191 (1992).
[32] E. M. Izhikevich, Int. J. Bifur. Chaos **10**, 1171 (2000).
[33] A. Sherman, Bull. Math. Biol. **56**, 811 (1994).
[34] A. Goldbeter, D. Gonze, G. Houart, J. Leloup, and J. Halloy, Chaos **11**, 247 (2001).
[35] Z. Yuan, J. Zhang, and T. Zhou, Phys. Rev. E **78**, 031901 (2008).
[36] Y. Setty, A. E. Mayo, M. G. Surette, and U. Alon, Proc. Natl. Acad. Sci. USA **100**, 7702 (2003).
[37] N. E. Buchler, U. Gerland, and T. Hwa, Proc. Natl. Acad. Sci. USA **100**, 5136 (2003).
[38] S. Mangan and U. Alon, Proc. Natl. Acad. Sci. USA **100**, 11980 (2003).
[39] T. S. Zhou, L. N. Chen, and K. Aihara, Phys. Rev. Lett. **95**, 178103 (2005).
[40] A. Koseska, E. Volkov, and J. Kurths, Europhys. Lett. **85**, 28002 (2009).
[41] A. Koseska, E. Ullner, E. Volkov, J. Kurths, and J. Gacía-Ojalvo, J. Theor. Biol. **263**, 189 (2010).
[42] A. Koseska, E. Volkov, and J. Kurths, Chaos **20**, 023132 (2010).
[43] P. Smolen, D. A. Baxter, and J. H. Byrne, Biophys. J. **83**, 2349 (2002).
[44] H. Song, P. Smolen, E. Av-Ron, D. A. Douglas, and J. H. Byrne, Biophys. J. **92**, 3407 (2007).